On the Reconfigurability of a Singly-Layered Dual-Band Reflectarray for Space Applications

Roger L. Farias[1] , Custódio Peixeiro[2] , Marcos V. T. Heckler[3]

[1]*Instituto de Soldadura e Qualidade, Oeiras, Portugal, rlfarias@isq.pt*
[2]*Instituto de Telecomunicações, Instituto Superior Técnico, Universidade de Lisboa, Lisbon, Portugal, custodio.peixeiro@lx.it.pt*
[3]*Universidade Federal do Pampa - Campus Alegrete, Alegrete, RS, Brazil, marcos.heckler@unipampa.edu.br*

Abstract— **This paper presents a feasibility study of a singly-layered dual-band reflectarray for space applications. The data links should operate simultaneously at K-band downlink frequency band 17.7-20.2 GHz with left-hand circular polarization (LHCP) and at Ka-band uplink frequency band 27-30 GHz with right-hand circular polarization (RHCP). The main aim is to present how a reflectarray can be designed so as to allow reconfigurability of its radiation pattern, especially in terms of beam steering to two different directions. The design is automated by means of a computational tool developed in MATLAB environment interfaced with the electromagnetic simulator CST Studio Suite by means of Visual Basic scripts. Simulation results are presented to demonstrate the efficiency of the proposed computational tool and reconfiguration strategy.**

Index Terms— Reflectarrays, Dual-Band Antennas, Reconfigurable Antennas, Space Antennas.

I. INTRODUCTION

In rural and isolated communities, where installation of internet providers may be economically unfeasible, people's daily life is severely affected by the lack of fast internet connections. This can be overcome by wireless links, whereby satellite communications can be an important alternative. Its features work as an important tool to connect anyone to everything and anywhere, and are essential to bridge the digital divide especially in developing countries [1].

In satellite communication systems, a high gain antenna is a basic requirement. Traditionally, two types of antennas are used: parabolic reflectors [2] and phased arrays [3]. Parabolic reflectors are particularly useful at high frequencies as the gain can be easily increased by increasing the electrical size of its aperture. In addition, the high radiation efficiency qualifies the parabolic reflector as a good candidate for satellite communications. The main drawback is its curved surface, which makes manufacturing challenging due to the expensive fabrication process and the large storage volume. These traits are critical due to the limited dimensions of satellites. To reduce the overall profile and manufacturing difficulties, microstrip antenna arrays, which are formed by many planar microstrip radiating elements, have been developed [4]. The main drawback is the feeding network that leads to high power loss for arrays with electrically large apertures. A compromise between the parabolic reflector and the microstrip array led to the development of microstrip reflectarray antennas [5], which consist of flat panels of printed scatterers, usually arranged in a square or circular aperture, and fed by a primary source (usually a horn antenna).

In order to emulate the operation of a curved reflector, patches of variable size, acting as reflecting elements with a controllable phase shift, are required to convert an incident spherical wave radiated by the feed into a reflected plane wave [6]. Due to the use of planar technology and the standard printed circuit board (PCB) manufacturing process, printed reflectarray antennas offer a good balance between conventional reflector antennas and phased arrays due to well-known advantages, such as low profile, light weight, compactness and low cost [5], [7]–[11]. Moreover, reflectarray antennas are gaining more and more attention in space satellite communication applications where new capabilities related to frequency, polarization and reconfigurability are needed [12]–[16].

Usually, two separate parabolic reflectors operating at different frequencies, one for the uplink and another for the downlink, are used to establish the communication between the Earth station and the satellite. For the sake of compactness, it is desirable to integrate these two antennas into a single aperture. This concept is not only aesthetically appealing, but also the size, the cost and the weight of the satellite antenna can be reduced if only one aperture is used for both bands. Furthermore, the capability of reflectarrays to implement independent phase distributions at different operating frequencies makes it possible to generate independent beams at different frequencies.

Many dual-band reflectarrays with linear and/or circular polarization have been reported in the literature. Single layer reflectarray designs have been presented previously. In [17], a single-layer unit-cell has been proposed for single-band operation and a reflectarray based on this unit-cell has been designed. Its performance for two fixed-beams and for a reconfigurable scenario has been assessed and numerical results are presented in [18]. A modified version of this unit-cell to extend the operation for two bands has been presented in [6]. The main advantage of this novel unit-cell is the share of the same aperture for both uplink and downlink in different frequency bands and with orthogonal circular polarizations. Up to now, the performance for a reconfigurable scenario for such an antenna was not investigated and, therefore, this is the main focus of this paper.

Due to the challenges and difficulties in the current state-of-the-art of reflectarray antennas, the main goal of this paper is to develop a computer-aided design (CAD) procedure for a low-cost single-layer printed reflectarray antenna with dual-band characteristics that allows reconfiguring its radiation pattern. The following specifications have been observed during the antenna design:

- The antenna should be dual-band dual-circularly polarized, in order to fulfill the requirements of typical satellite communication systems and thus increase its functionality.
- Investigation of the feasibility by simulations of a single-layer dual-band circularly polarized reflectarray employing RF-switches, such as PIN diodes, to obtain beam steering capability aiming to cover different regions on Earth.

In the next section, the application scenario and the basic design strategy for the unit-cell to allow reconfigurability is presented. In section III, the software developed for the automated reflectarray design is described. The performance assessment is presented in section IV. Finally, the conclusion is given in section V.

II. APPLICATION SCENARIO AND REFLECTARRAY DESIGN

A potential application scenario is the Brazilian Geostationary Satellite for Defense and Strategic Communications (SGDC), launched in 2017. The data links should operate simultaneously at K-band

---- Downlink (17.7 – 20.2 GHz) – Left-handed circular polarization (LHCP)
---- Uplink (27 – 30 GHz) – Right-handed circular polarization (RHCP)
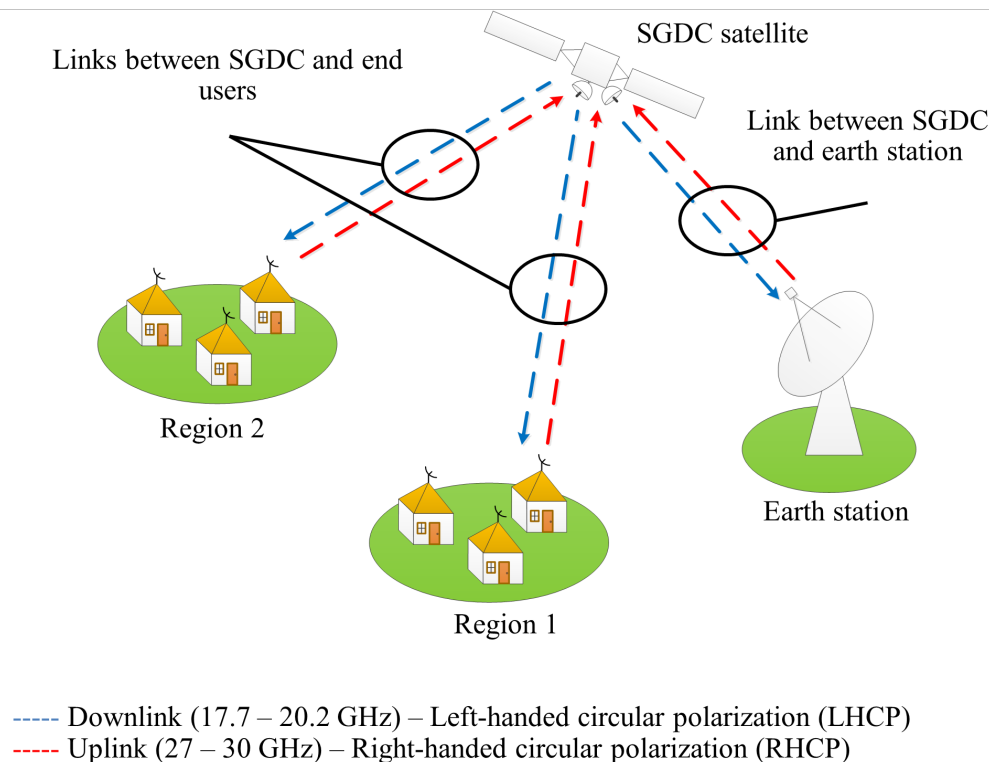
Fig. 1. Schematic view of a hypothetical application scenario.

downlink frequency band 17.7-20.2 GHz and at Ka-band uplink frequency band 27-30 GHz. Left-hand circular polarization (LHCP) is used for the downlink, whilst RHCP is used for the uplink. One of the tasks of this satellite is to provide internet coverage in the Amazon Rain Forest in Northern Brazil. Another task is to enable strategic communication links between that region and Brazil's capital Brasília, located roughly at latitude $15° \, 47' \, 38'' \, S$ and longitude $47° \, 52' \, 58'' \, W$. This is schematically shown in Fig. 1. Due to the position of this satellite in the sky over Brazil and the geographic locations mentioned above, four different beam steering situations may occur (angles are given from the antenna boresight):

- Both uplink and downlink beams should point to $18.2°$;
- K-band beam pointing to $9.1°$ and Ka-band beam pointing to $18.2°$;
- K-band beam pointing to $18.2°$ and Ka-band beam pointing to $9.1°$;
- Both uplink and downlink beams pointing to $9.1°$.

The reflectarray design is based on the unit-cells presented in [18] and [6], which is schematically shown in Figure 2(a). To enable beam steering capability with a one-bit reconfiguration scheme, the stub delay-lines are split into two section with a gap length $g = 0.25$ mm, as illustrated in Figure 2(b). On this gap, any kind of RF-switch (such as PIN-diodes) can be soldered, so as to allow varying the electrical size of the stubs and, consequently, to vary the phase of the back-scattered field. For operation at K-band, the spiral stub 1 (L_{K1}) is connected to the outer circular ring, whereas the spiral arc stub 2 (L_{K2}) forms an isolated section when the PIN-diode is set to OFF-state. Both arcs become continuous when the PIN-diode is set to ON-state. For operation at Ka-band, the stub 1 (L_{Ka1}) is connected to the inner circular ring, whereas the stub 2 (L_{Ka2}) forms an isolated stub when the PIN-diode is set
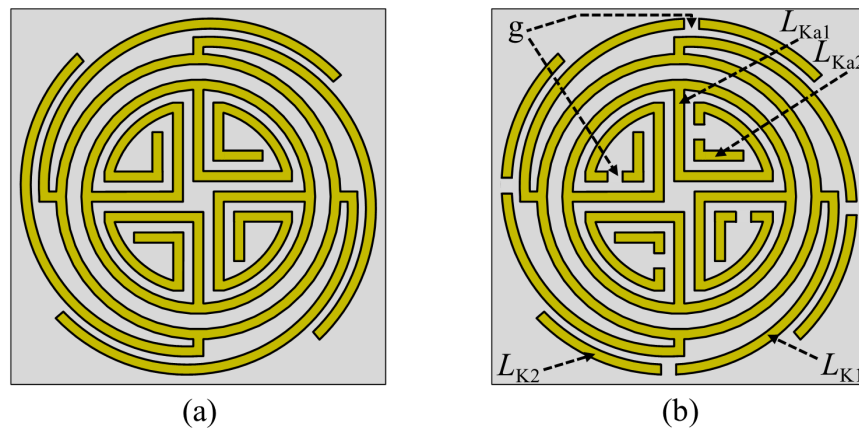
Fig. 2. Schematic top views: (a) original unit-cell for fixed-beam applications; (b) reconfigurable unit-cell.

to OFF-state and form a continuous stub when the switch is set to ON-state. For the reconfigurability assessment presented in this paper, the switches are replaced by ideal short and open circuits for ON and OFF-states, respectively.

The laminate Rogers Duroid 5880 has been considered for this design and presents the following parameters: thickness $h = 1.575$ mm, dielectric constant $\varepsilon_r = 2.2$ and loss tangent $\tan \delta = 0.0012$ at 20 GHz and $\tan \delta = 0.0015$ at 30 GHz. The analysis of the unit cell has been carried out by setting up a periodic boundary condition along with Floquet excitation in CST Microwave Studio.

The effect of the incident angle θ_{inc}, i.e. the effect of the impinging wave upon the unit-cell surface, on the reflected phase and magnitude curves was obtained at both central frequencies and the results are shown in Figs. 3 and 4 as a function of the length of the phase-delay lines. In the K-band, the curves indicate that, for $\theta_{inc} \leq 30°$, the phase is almost the same as for normal incidence and the amplitude is larger than -0.6 dB. For $\theta_{inc} = 40°$, the maximum phase deviation from the other curves is lower than $46°$. In the Ka-band, the maximum phase deviation is lower than $60°$. The magnitude response of the scattered field presents values larger than -0.9 dB in both bands for $\theta_{inc} = 40°$.
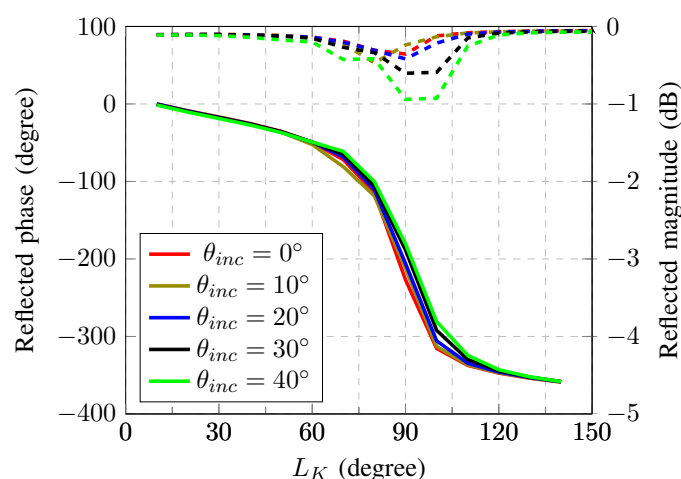
Fig. 3. Reflected phase (solid) and magnitude (dashed) responses versus the length of phase delay-lines under different incidence angles at 18.95 GHz.

With the unit-cell described above, a reflectarray with 20×20 elements has been designed. The
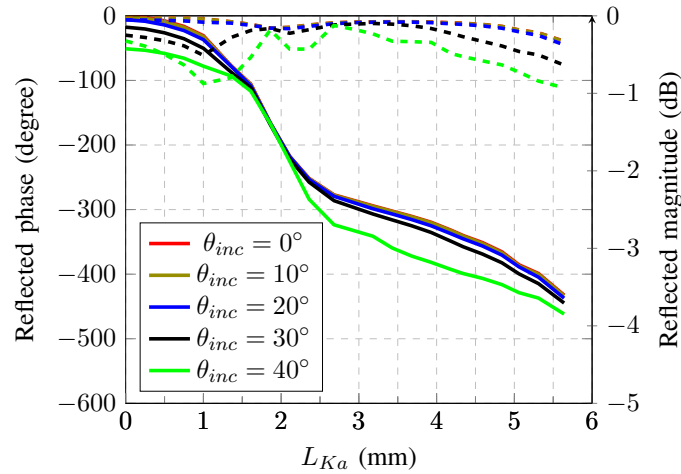
Fig. 4. Reflected phase (solid) and magnitude (dashed) responses versus the length of phase delay-lines under different incidence angles at 28.5 GHz.

cells are uniformly spaced in both aperture dimensions by 5.45 mm, which is equivalent to $0.34 \lambda_0$ at 18.95 GHz and $0.52 \lambda_0$ at 28.5 GHz; hence the resulting square aperture exhibits an edge size of 109 mm. The planar reflector is centered at the origin of a rectangular coordinate system, where the z-axis is positioned normally to the reflector aperture. The phase center of the feed horn for both K and Ka-bands has been set in the position (-15.02, 0, 93.8) mm above the reflectarray surface. The radiation pattern of both horns has been modelled using a $\cos^q \theta$ function, where $q = 6.8$ at 18.95 GHz and $q = 7$ at 28.5 GHz. The illumination level at the reflectarray edges is around -8.8 dB and -9.1 dB at 18.95 and 28.5 GHz, respectively. These values are chosen as a trade-off between gain, side lobe level and spillover efficiency.

The reflectarray aperture was illuminated by two commercial linearly polarized (LP) standard horn antennas (mod 20240-15 and 22240-15 from Flann Microwave): one operating at K-band and the other at Ka-band. Both horns have been modelled in CST. Due to the use of linearly polarized horns, the simulations using the time domain solver were performed with each horn in two orthogonal orientations. Circularly polarized feeders can be then emulated by post-processing. Both LHCP and RHCP radiation patterns propagating towards the positive z direction may be written as

$$E_{\text{LHCP}} = \frac{E_\theta^x + E_\theta^y - jE_\phi^x - jE_\phi^y}{2} \qquad (1)$$

$$E_{\text{RHCP}} = \frac{E_\theta^x + E_\theta^y + jE_\phi^x + jE_\phi^y}{2} \qquad (2)$$

where E_θ^x and E_ϕ^x are the LP components for a x-polarized feed and E_θ^y and E_ϕ^y are the LP components for a y-polarized feed. Thus, considering an incident ideal RHCP wave radiated by the feed horn $(\vec{E}^x + j\vec{E}^y)$ propagating towards the negative z-direction, equations (1) and (2) provide LHCP and RHCP radiation patterns defined as the co-polarized and cross-polarized components, respectively. Similarly, considering an incident ideal LHCP wave radiated by the feed horn $(\vec{E}^x - j\vec{E}^y)$ propagating towards the negative z-direction, equations (1) and (2) provide LHCP and RHCP radiation patterns defined as the cross-polarized and co-polarized components, respectively. Therefore, this was the way how the circular polarization was achieved.
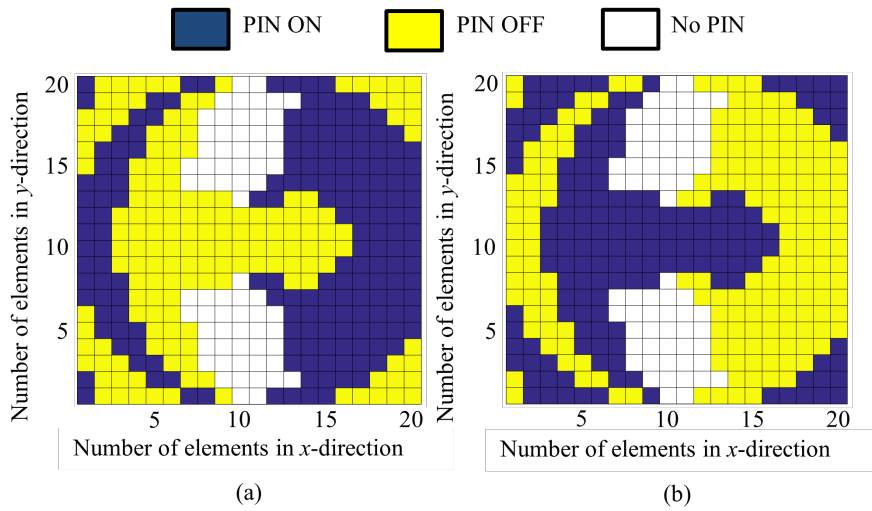
Fig. 5. States of the PIN diodes of the dual-band reflectarray operating at K-band: (a) Beam 1; (b) Beam 2.
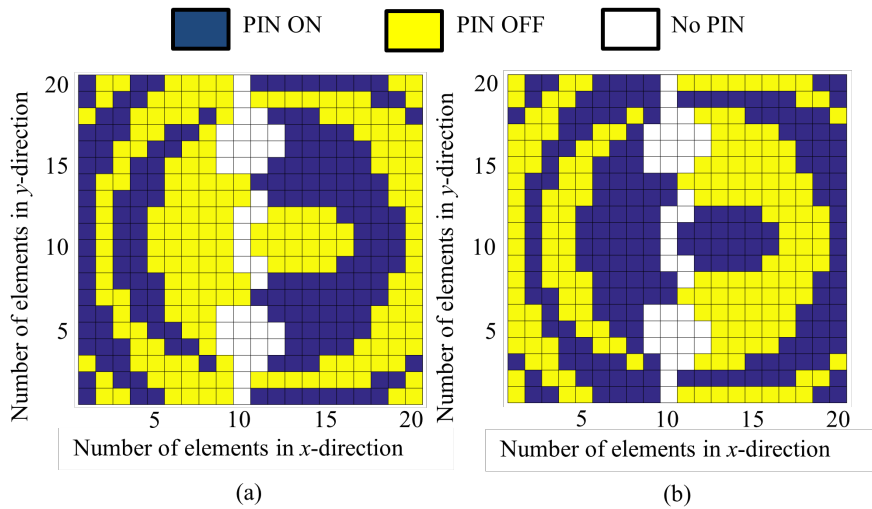
Fig. 6. States of the PIN diodes of the dual-band reflectarray operating at Ka-band: (a) Beam 1; (b) Beam 2.

Regarding the states of the PIN diodes for each element, they can be determined from the needed phase shift, which can be calculated from

$$\phi_{E\,mn}^{(j)} = k_0 \left[d_{mn} - \left(x_{mn} \cos \phi_b^{(j)} + y_{mn} \sin \phi_b^{(j)} \right) \sin \theta_b^{(j)} \right], \qquad (3)$$

where k_0 is the propagation constant in free space, d_{mn} is the distance from the phase center of the feed horn to the center of the mn-th cell, x_{mn} and y_{mn} are the coordinates of the position of the mn-th element in the reflectarray aperture with respect to the origin of the coordinate system, and $\theta_b^{(j)}$ and $\phi_b^{(j)}$ indicate the desired main beam direction j. The resulting distributions of the PIN diodes states on the reflactarray aperture are illustrated in Fig. 5 for 18.95 GHz and Fig. 6 for 28.5 GHz. For the two radiation patterns to yield satisfatory beam pointing, it is important to properly choose the ON and OFF states of each unit-cell during the design process of the reflectrarray. The beams should point to $(\theta_b^{(1)} = 9.1°, \phi_b^{(1)} = 0°)$ for $j = 1$ and to $(\theta_b^{(2)} = 18.2°, \phi_b^{(2)} = 0°)$ for $j = 2$.

The ON/OFF state of the PIN diodes on each element is determined by the magnitude of $\phi_{E\,mn}^{(j)}$. If

$\left|\phi_{E\,mn}^{(1)}\right| < \left|\phi_{E\,mn}^{(2)}\right|$, the PIN diode is ON for beam 1 and OFF for beam 2. Similarly, the PIN diode is OFF for beam 1 and ON for beam 2 if the condition $\left|\phi_{E\,mn}^{(1)}\right| > \left|\phi_{E\,mn}^{(2)}\right|$ applies. If $\left|L_K^{(1)} - L_K^{(2)}\right| <$ 0.25 mm or if $\left|L_{Ka}^{(1)} - L_{Ka}^{(2)}\right| < 0.25$ mm, then the unit-cells are not loaded with PIN diodes, because the gap length $g = 0.25$ mm is shorter than the required additional stub length.

The phase compensation is calculated for each desired beam steering direction and for each band independently. This makes every unit-cell unique, since each one will present different stub lengths and, consequently, the gap will be placed in different positions. Therefore, reconfigurability is achieved with 400 unit-cells with distinct stub lengths, which is impracticable to be drawn manually in the electromagnetic simulator. This process has been automatized by means of a code written in MATLAB, so as to generate the geometry of the reflectarray and to export it to CST Studio Suite. The details of this code are given in the next section.

III. REFLECTARRAY SIMULATOR

This section is dedicated to the explanation of the algorithm which automates the reflectarray assembly step by step and includes the reflection coefficients information of the unit-cell evaluated with CST Studio Suite. The reflectarray simulator is a code that combines both MATLAB and CST Studio Suite, which are interfaced using visual basic scripts. In contrast to other papers found in the literature, such as [19] and [20], which aim the generation of the geometry of single-band reflectarrays automatically, the present work proposes an algorithm that automates the creation of the electromagnetic model for a reconfigurable dual-band reflectarray. It automates the generation of the antenna model in CST Studio Suite, so as to reduce the laborious effort of drawing hundreds of antenna elements manually. Besides taking significant time, creating the electromagnetic model of very large reflectarrays is strongly susceptible to human errors. Furthermore, it allows estimating the radiation pattern performance of the reflectarray antenna prior to the execution of a full-wave simulation.

The flowchart of the reflectarray simulator algorithm is presented in Fig. 7. The processes running in MATLAB are represented by the blue elements and those to be executed in CST Studio Suite are given in red. The reflectarray simulator is capable of producing different kinds of radiation patterns, which can be divided as follows:

- Ideal radiation pattern: the magnitude of the reflection coefficient is supposed to be equal to 1 (0 dB) for all the unit-cells composing the reflectarray, so that the impinging wave on the reflectarray surface is completely reflected; i.e. it does not take losses into account;
- Radiation pattern with losses: the real characteristics of the materials (losses) and the phase errors related to the simplification of the incident angles of the wave impinging upon each unit-cell are considered. In this case, the reflectarray simulator will provide more accurate results in a simple way, hence providing good engineering predictions that are closer to the pattern calculated with full-wave approaches.

In the first step of the algorithm, the tool requires only the input parameters to complete the calculation. The mandatory input parameters are: feed definition, number of elements, beam direction and operating frequency. The description for these parameters is shown in Table I. They are used to optimize the aperture efficiency, with illumination tapering around -10 dB and maximum angle of incidence at the array edges of approximately $40°$. The phase distribution is calculated so as to produce the required focused beam. The necessary phase shift at each unit-cell is obtained by varying one or
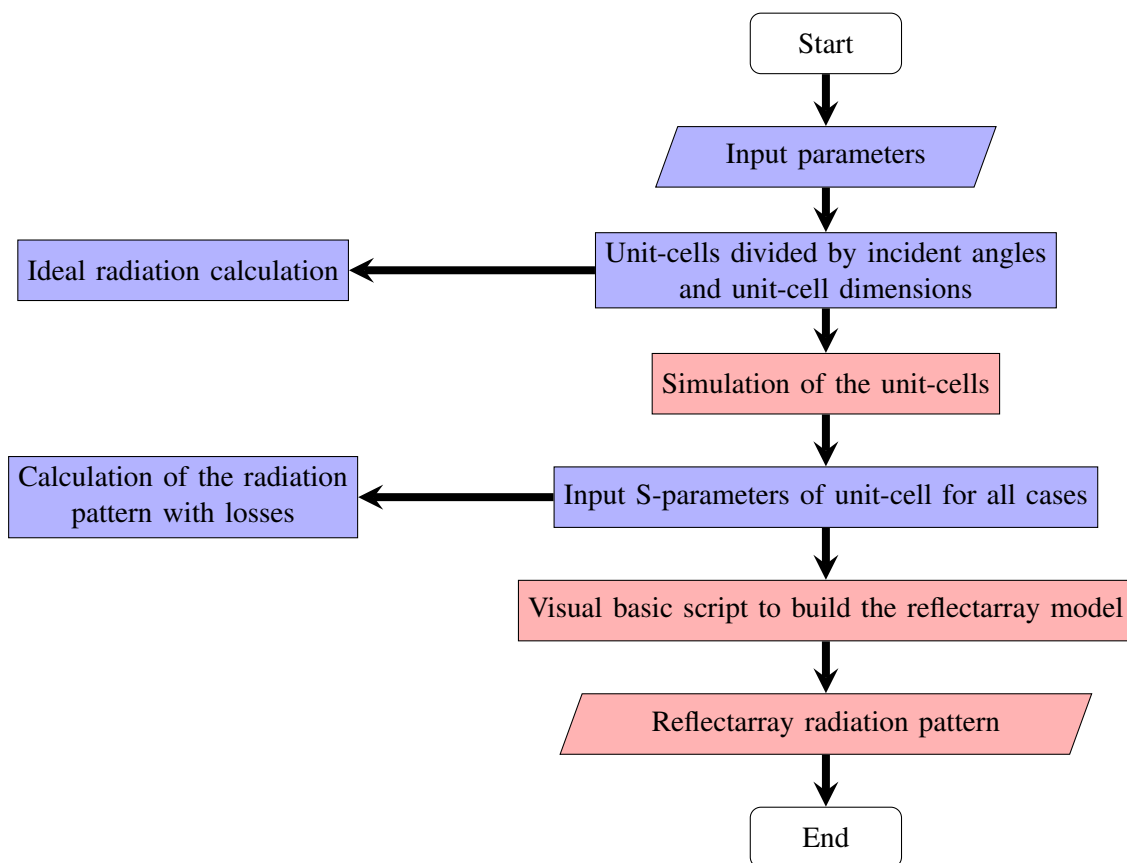
Fig. 7. Flowchart of the algorithm to design the dual-band reconfigurable reflectarray: in blue are the processes run in MATLAB; in red are the routines executed with CST Studio Suite.

several geometric parameters. Additionally, the phase distribution over the reflectarray surface is closely related to the feed and scatterer positions. In this way, the required phase shift $\phi_{E\,mn}^{(j)}$ will depend on the unit-cell parameters and on the angle of incidence of the impinging wave. Thus, the unit-cells of the reflectarray have been classified according to their geometrical parameters and the local angle of incidence.

Parameter	Description
Feed definition	x_F, y_F, z_F (mm): coordinates of the feed position.
	q: feed power pattern which is modelled as $\cos^q \theta_F$.
Number of elements	N_x, N_y: number of elements of the reflectarray in the x and y axis, respectively.
Distance between cells	d_x, d_y (mm): x and y dimensions of the periodic cell. Preferably values around 0.5 lambda to prevent grating lobes.
Beam direction	θ_b, ϕ_b: the desired main beam direction, in degrees.
Operating frequency	f (GHz): central frequency.

TABLE I. Description of input parameters for the dual-band reconfigurable reflectarray simulator.

In the second step of the algorithm, all the unit-cells are fit into cases where the angle of incidence and the variable parameter of phase-shift change. In this case, the angle of incidence on the reflectarray aperture varies between 0° and 40°; for this variation, a 10° step (5 cases) has been considered. The phase-shift range for the K-band has been considered to be between 10° and 150° with a 10° step (15 cases). For the Ka-band, this parameter has been varied in the range between 0.25 mm and 5.5 mm with

a 0.25 mm step (22 cases). This leads to $5 \times 15 = 75$ different unit-cell simulations in the lower band and $5 \times 22 = 110$ in the higher band. The steps for these parameters could have been made smaller, but the values assumed here already provide sufficiently accurate results. For the sake of clarity, the required values between the mentioned steps have been estimated by means of interpolation. The unit-cell has been then simulated for these 185 cases, where periodic boundary condition was used at the four lateral walls. A Floquet port was assigned to excite two orthogonal Floquet modes (TE and TM) with different incident angles. With the correct combination between these modes, circularly polarized waves can be produced, which is necessary for the proposed application: RHCP in the K-band and LHCP in the Ka-band [17], [18]. The main inaccuracy of this approach arises from the periodic boundary conditions, which yields an infinite two-dimensional periodic array environment. Additionally, it is worthwhile to mention that local periodicity assumption implicates that all elements are considered to be identical, which is not typically true in the case of reflectarrays. As a result, the mutual coupling is considered to be the same for all elements in the array, which holds only as approximated values of mutual coupling.

In the third step of the algorithm, the unit-cell is simulated in CST Studio Suite considering all the geometric details, such as dimensions and substrate properties. Then, a file of all the reflection coefficients (magnitude and phase) of the unit-cell for the cases stated above is generated. The reflection curves generated by using CST Studio Suite are added into the reflectarray simulator as an input file, hence allowing to take into account the material losses as well as the phase error compensation. According to the different reflection phase values and incident angle data, the reflectarray simulator allows to define the locations of the unit-cells on the reflectarray surface as well as the dimensions of the radiating element which corresponds to an approximate level of $\phi_{E_{mn}}$ in equation (3).

As the last step of the algorithm, when the set of dimensions is known, the reflectarray simulator generates a script based on visual basic and the reflectarray geometry can be generated in the CST Studio Suite. After this step, the designer needs only to configure the simulation setup by setting the simulation frequency, the material specifications and the feed horn model.

IV. PERFORMANCE ASSESSMENT OF THE DESIGNED REFLECTARRAY

The phase distributions associated with the selected application scenario (section II) are shown in Figs. 8-10 and the corresponding radiation pattern results are shown in Fig. 11. Good overall performance can be verified, since the main beams have been pointed to the respective desired directions. This flexibility to achieve different main beam pointing directions is very important for satellite communication applications.

The simulated gain patterns of the dual-band circularly polarized reflectarray antenna at K and Ka bands for both off-broadside steered beams at $(\theta_b^{(1)} = 9.1°, \phi_b^{(1)} = 0°)$ and $(\theta_b^{(2)} = 18.2°, \phi_b^{(2)} = 0°)$ are depicted in Figs. 12 and 13.

From Figs. 12(a), (c) and (e), it is observed that the gain patterns for main beam 1 focus in the direction $(\theta_b^{(1)} = 9.1°, \phi_b^{(1)} = 0°)$ in the whole K-band, as desired. At 18.95 GHz, the simulated peak gain is 23.82 dBic with cross-polarization decoupling (XPD) equal to 26.16 dB. The side lobe level (SLL) is 15.03 dB and the maximum aperture efficiency at 18.95 GHz for beam 1 is 40.44 %. From Figs. 12(b), (d) and (f), it is noticeable that the gain patterns for main beam 2 exhibit also maximum level in the intended direction $(\theta_b^{(2)} = 18.2°, \phi_b^{(2)} = 0°)$ in the whole K-band. At 18.95 GHz, the simulated peak gain is 23.93 dBic with $XPD = 25.24$ dB and $SLL = 17.15$ dB. Furthermore, the maximum aperture efficiency at 18.95 GHz for beam 2 is 41.48 %.
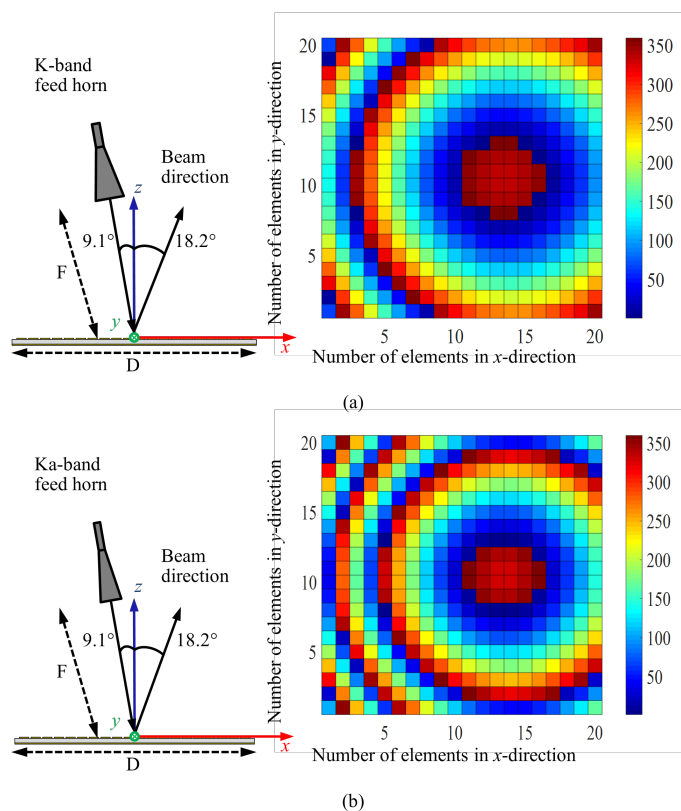
Fig. 8. Required phase distributions to steer the main beam to (a) $\theta_{max} = 18.2°$ from the boresight at 18.95 GHz; and (b) $\theta_{max} = 18.2°$ from the boresight at 28.5 GHz.

The curves presented in Figs. 13(a), (c) and (e) show that the gain patterns of main beam 1 can be successfully steered to the direction $(\theta_b^{(1)} = 9.1°, \phi_b^{(1)} = 0°)$ in the whole Ka-band, as desired. At 28.5 GHz, the simulated peak gain is 28.39 dBic, with the largest side lobe level being 16.87 dB. Polarization purity is also very good, since $XPD = 24.23$ dB, and the maximum aperture efficiency at 28.5 GHz for beam 1 yielded 51.26 %. From Figs. 13(b), (d) and (f), one can verify that the main beam has been pointed to the intended direction $(\theta_b^{(2)} = 18.2°, \phi_b^{(2)} = 0°)$ in the whole Ka-band and with simulated peak gain of 28.44 dBic at 28.5 GHz. The cross-polarization decoupling obtained is 25.25 dB and the largest side lobe is 18.59 dB. Moreover, the maximum aperture efficiency at 28.5 GHz for beam 2 is 51.85 %.

Figs. 14 and 15 show the simulated gain and AR versus frequency at K and Ka-band for the two beams. According to Fig. 14, the simulated 3-dB gain and AR bandwidths of both beams yield values larger than 23.75 %, which is equivalent to the specified K-band (16.7 – 21.2 GHz). Regarding Fig. 15, the simulated 3-dB gain and AR bandwidths of both beams yield values larger than 17.54 %, which is equivalent to the complete desired Ka-band (26 – 31 GHz). Finally, it is worthwhile to notice that the axial ratio levels remained lower than 1.2 dB for both beams at both K- and Ka-bands. This reinforces the remarkable performance of the unit-cell described in [6] and the proposed computer-aided dual-band reconfigurable reflectarray design procedure presented in this paper.
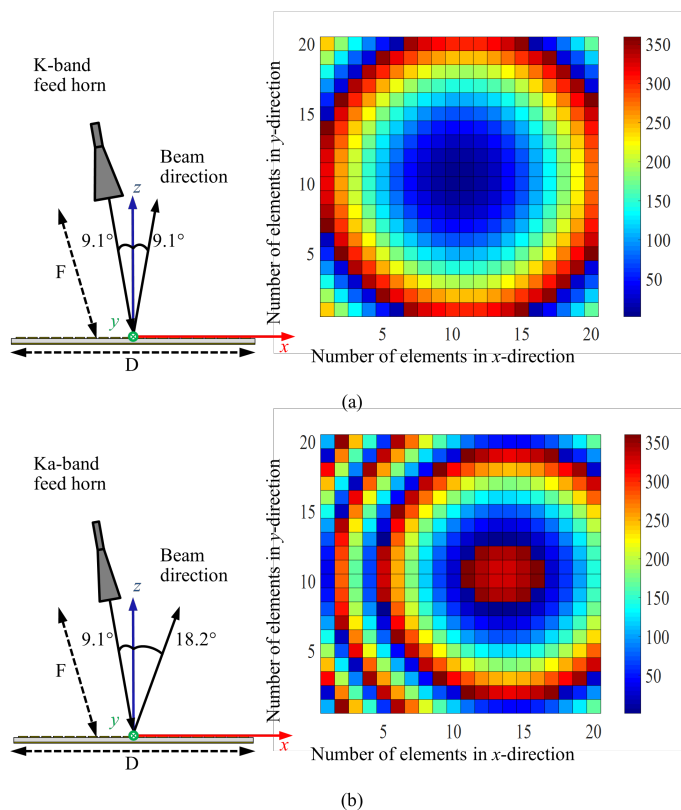
Fig. 9. Required phase distribution for each element to (a) $\theta_{max} = 9.1°$ from the boresight at 18.95 GHz; and (b) $\theta_{max} = 18.2°$ from the boresight at 28.5 GHz.
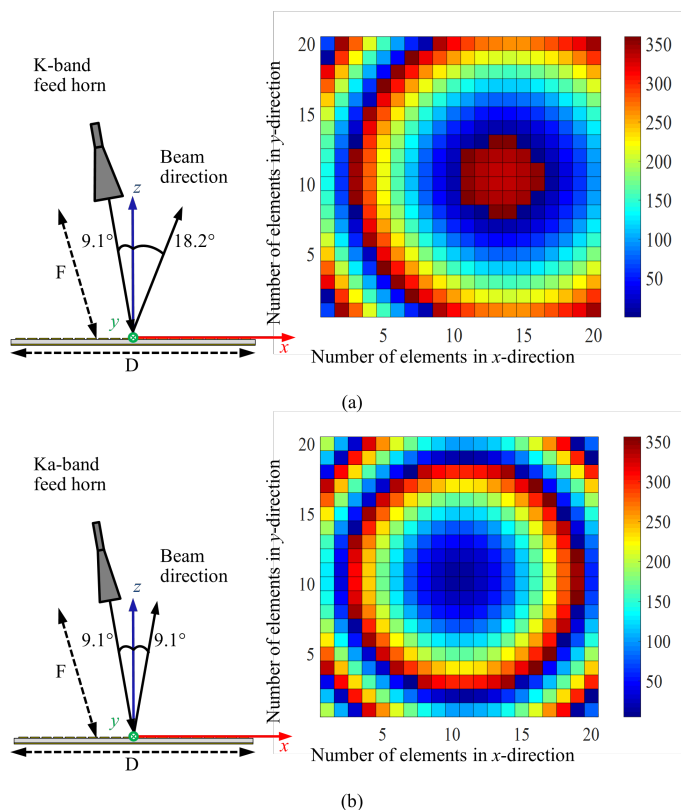
Fig. 10. Required phase distribution for each element to (a) $\theta_{max} = 18.2°$ from the boresight at 18.95 GHz; and (b) $\theta_{max} = 9.1°$ from the boresight at 28.5 GHz.
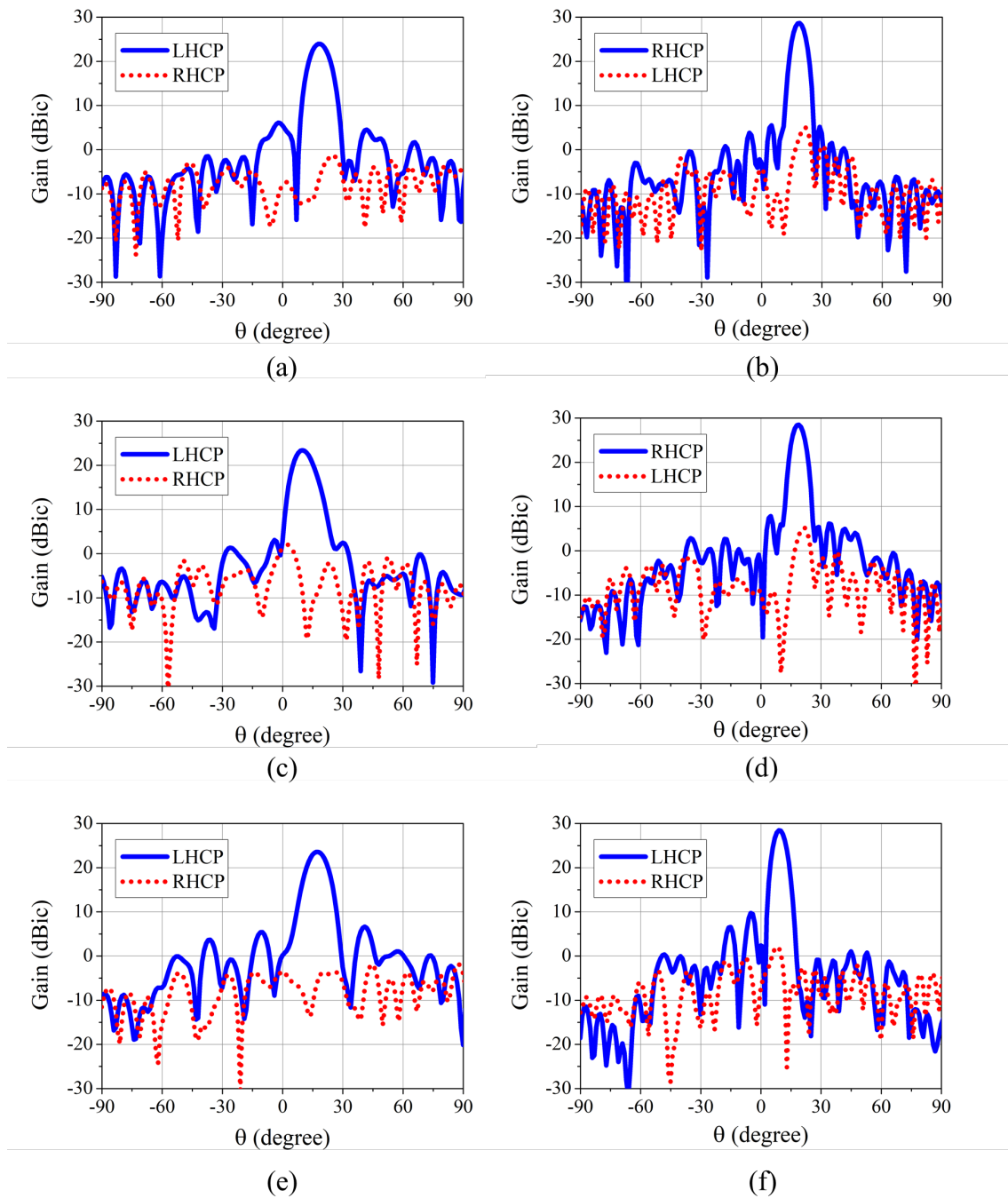
Fig. 11. Simulated radiation pattern results (gain scale) of the proposed antenna at 18.95 GHz and 28.5 GHz: (a) Beam pointing to 18.2° at 18.95 GHz; (b) Beam pointing to 18.2° at 28.5 GHz; (c) Beam pointing to 9.1° at 18.95 GHz; (d) Beam pointing to 18.2° at 28.5 GHz; (e) Beam pointing to 18.2° at 18.95 GHz; (f) Beam pointing to 9.1° at 28.5 GHz.
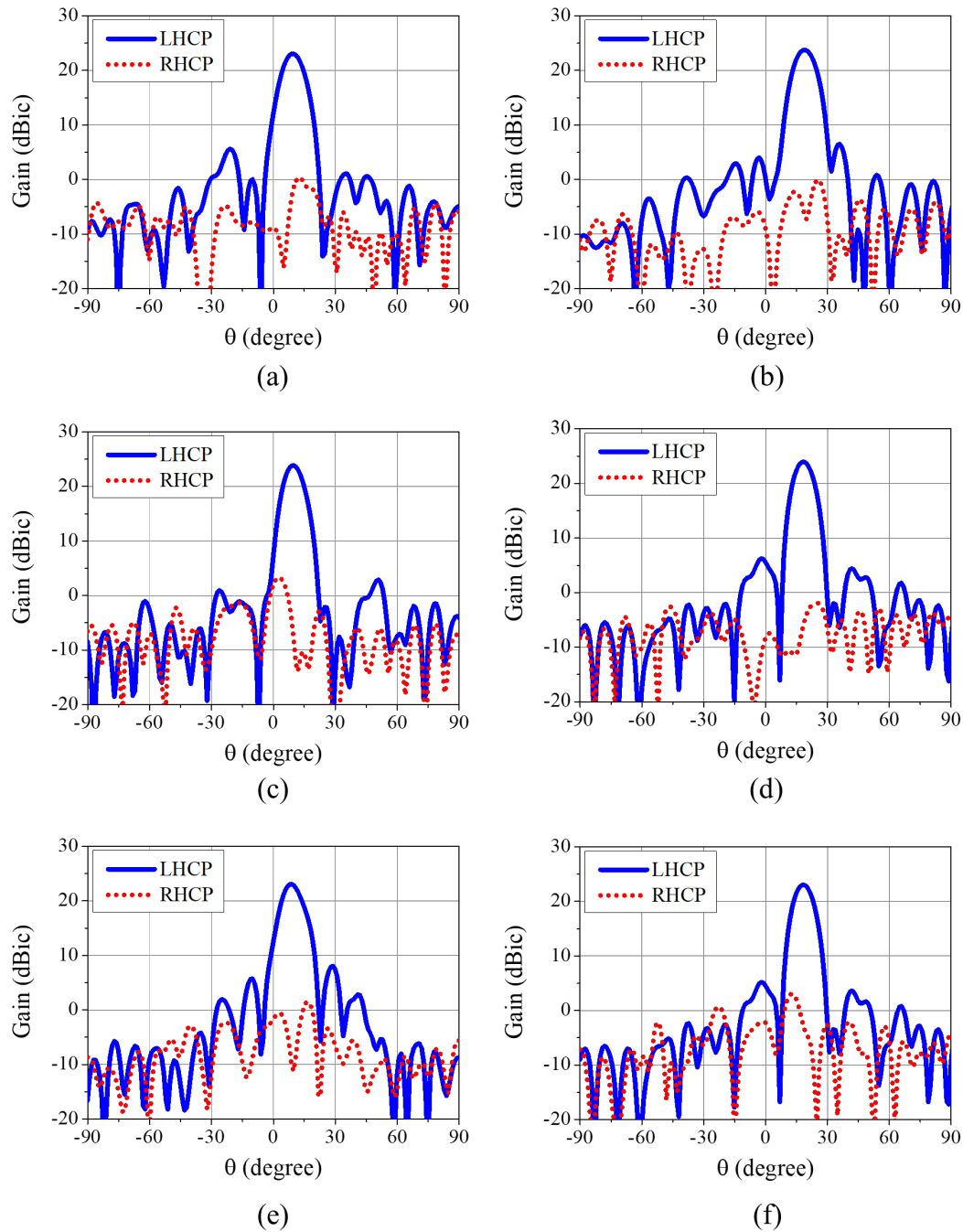
Fig. 12. Radiation pattern results for the K-band: (a) Beam 1 at 17.70 GHz; (b) Beam 2 at 17.70 GHz; (c) Beam 1 at 18.95 GHz; (d) Beam 2 at 18.95 GHz; (e) Beam 1 at 20.2 GHz; (f) Beam 2 at 20.2 GHz.
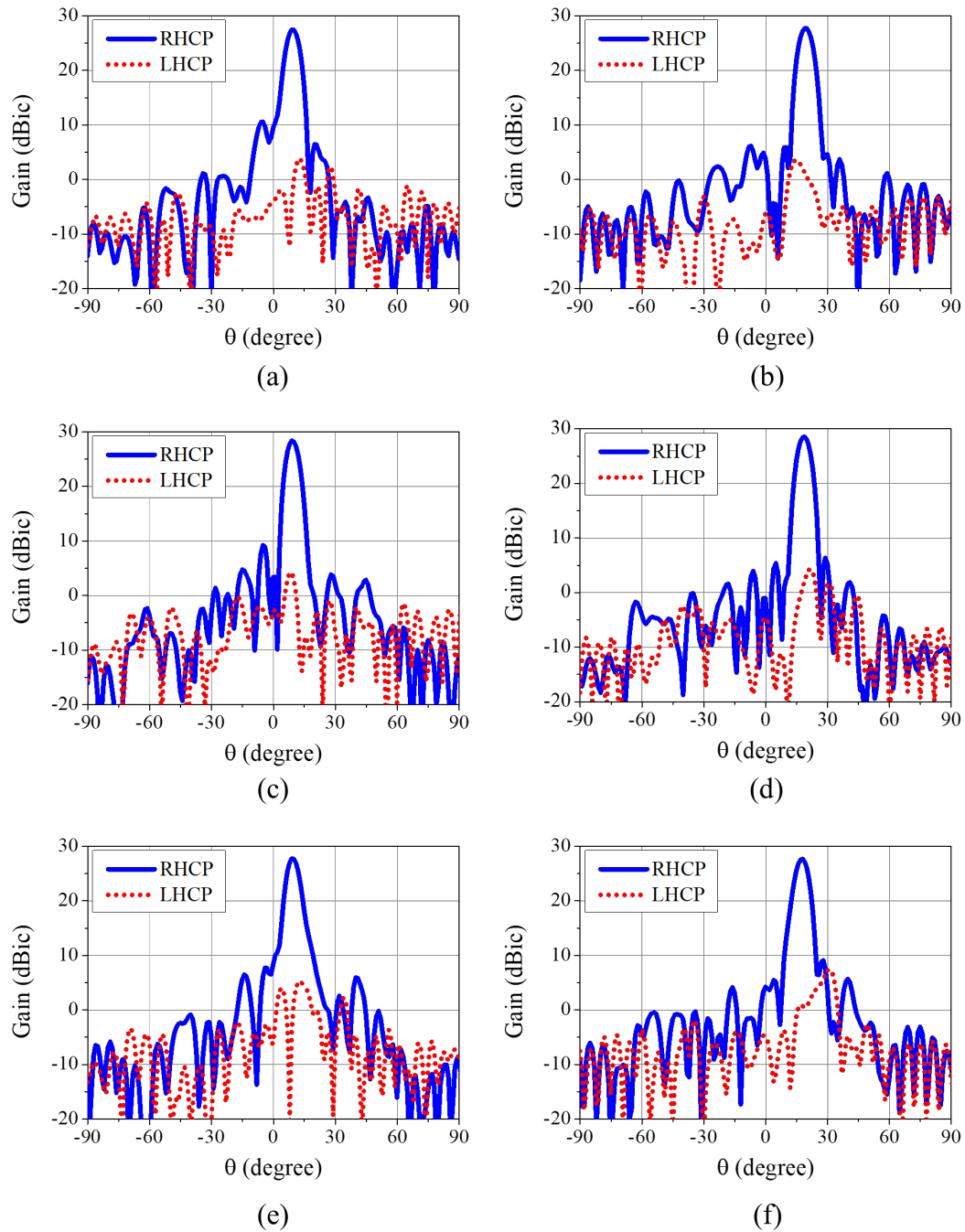
Fig. 13. Radiation pattern results for the Ka-band: (a) Beam 1 at 27.0 GHz; (b) Beam 2 at 27.0 GHz; (c) Beam 1 at 28.5 GHz; (d) Beam 2 at 28.5 GHz; (e) Beam 1 at 30.0 GHz; (f) Beam 2 at 30.0 GHz.
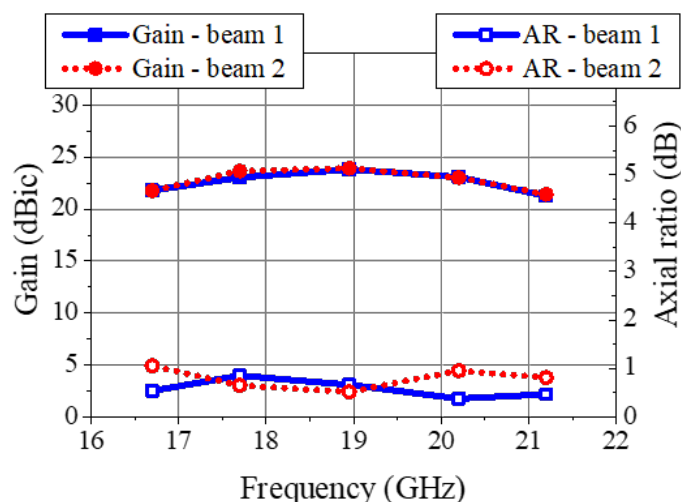
Fig. 14. Simulated gain and AR versus the K frequency band for beams 1 and 2.
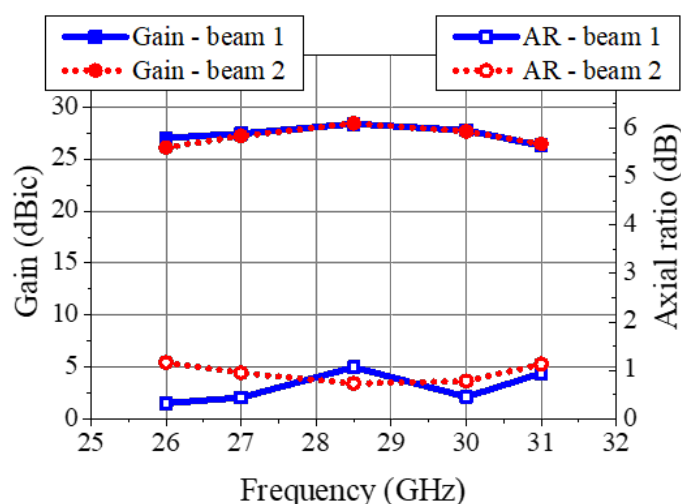
Fig. 15. Simulated gain and AR versus the Ka frequency band for beams 1 and 2.

V. Conclusion

In this paper, a computer-aided design procedure and the performance assessment of a low-cost dual-band dual-circularly polarized reflectarray antenna operating at two frequency bands namely from 17.7 to 20.2 GHz (K-band) and from 27 to 30 GHz (Ka-band) have been presented. The reflectarray antenna unit-cell has the advantage of being a single layer dual-circularly polarized structure which enables the reflectarray to operate with dual-linear polarization as well. It should be highlighted that since the required phase-shift of the unit-cell at each frequency band depends on only one parameter, the reflectarray design is very simple [6].

The reflectarray reconfigurability has been obtained by switching its main beam pointing direction between 9.1° and 18.2° from boresight in both K- and Ka-bands. A 1-bit discretization yielded accepta-ble results to change the main beam pointing direction. The proposed approach for reconfigurability can be generalized to the use of more pin-diodes per unit-cell as well, hence allowing more beams (beam steering) or changing the shape of the radiation pattern (beam shaping). Moreover, the computer-aided

design procedure presented in this paper was able to simplify the laborious task of building the entire reflectarray as well as speeding up its analysis and its design.

ACKNOWLEDGEMENTS

REFERENCES

[1] ITU, "Evolving satellite communications," 2019, available in https://www.itu.int/en/itunews/Documents/2019/2019-02/2019_ITUNews02-en.pdf.

[2] C. Balanis, *Modern Antenna Handbook*. John Wiley & Sons, 2007.

[3] R. Mailloux, *Phased Array Antenna Handbook*. Artech House, 2005.

[4] R. Mailloux, J. McIlvenna, and N. Kernweis, "Microstrip array technology," *IEEE Trans Antennas Propag*, vol. 29, no. 1, pp. 25–37, 1981.

[5] J. Huang, "Microstrip reflectarray," in *Antennas and Propagation Society Symposium 1991 Digest*, vol. 2, pp. 612–615, June 24-28 1991.

[6] R. L. Farias, C. Peixeiro, and M. V. T. Heckler, "Single-layer dual-band dual-circularly polarized reflectarray for space communication," *IEEE Trans Antennas Propag*, vol. 70, no. 7, pp. 5989–5994, 2022.

[7] J. Huang and J. Encinar, *Reflectarray Antennas*. Wiley-IEEE Press, 2007.

[8] J. Shaker, M. Chaharmir, and J. Ethier, *Reflectarray Antennas: Analysis, Design, Fabrication and Measurement*. John Wiley & Sons, 2013.

[9] N. Payam, Y. Fan, and Z. Atef, *Reflectarray Antennas: Theory, Designs, and Applications*. John Wiley & Sons, 2018.

[10] D. Pozar, S. Targonski, and H. Syrigos, "Design of millimeter wave microstrip reflectarrays," *IEEE Trans Antennas Propag*, vol. 45, no. 2, pp. 287–296, 1997.

[11] F. Tsai and M. Bialkowski, "Designing a 161-element ku-band microstrip reflectarray of variable size patches using an equivalent unit cell waveguide approach," *IEEE Trans Antennas Propag*, vol. 51, no. 10, pp. 2953–2962, 2003.

[12] E. Martinez-de Rioja, D. Martinez-de Rioja, J. A. Encinar, A. Pino, B. Gonzalez-Valdes, Y. Rodriguez-Vaqueiro, M. Arias, and G. Toso, "Advanced multibeam antenna configurations based on reflectarrays: Providing multispot coverage with a smaller number of apertures for satellite communications in the K and Ka bands," *IEEE Antennas and Propagation Magazine*, vol. 61, no. 5, pp. 77–86, 2019.

[13] D. Martinez-de Rioja, R. Florencio, E. Martinez-de Rioja, M. Arrebola, J. A. Encinar, and R. R. Boix, "Dual-band reflectarray to generate two spaced beams in orthogonal circular polarization by variable rotation technique," *IEEE Transactions on Antennas and Propagation*, vol. 68, no. 6, pp. 4617–4626, 2020.

[14] J.-M. Baracco, P. Ratajczak, P. Brachat, J.-M. Fargeas, and G. Toso, "Ka-band reconfigurable reflectarrays using varactor technology for space applications: A proposed design," *IEEE Antennas and Propagation Magazine*, vol. 64, no. 1, pp. 27–38, 2022.

[15] Y.-H. Nam, Y. Kim, S.-G. Lee, and J.-H. Lee, "Hybrid reflectarray antenna of passive and active unit cells for highly directive two-direction beam steering," *IEEE Access*, vol. 11, pp. 6299–6304, 2023.

[16] J. Hu, P.-L. Chi, and T. Yang, "Novel 1-bit beam-scanning reflectarray with switchable linear, left-handed, or right-handed circular polarization," *IEEE Transactions on Antennas and Propagation*, vol. 71, no. 2, pp. 1548–1556, 2023.

[17] R. Farias, C. Peixeiro, M. Heckler, and E. Schlosser, "Axial ratio enhancement of a single-layer microstrip reflectarray," *IEEE Antennas Wireless Propag Lett*, vol. 18, pp. 2622–2626, 2019.

[18] R. Farias, C. Peixeiro, and M. Heckler, "Performance assessment of a reconfigurable circularly polarized reflectarray at K-band," in *14th European Conference on Antennas and Propagation - EuCAP 2020*, March, 2020.

[19] M. N. B. Zawawi, "New antenna for millimetre wave radar," Ph.D. dissertation, Université Nice Sophia Antipolis, 2015.

[20] S. A. M. Solimam, A. M. Attiya, and Y. M. Antar, "Low profile/single layer X-band circularly polarized reflectarray with a linearly polarized feed," *Progress In Electromagnetics Research M*, vol. 113, pp. 87–99, 2022.